A&A 541, L10 (2012)
DOI: 10.1051/0004-6361/201219303

Astronomy & Astrophysics

Letter to the Editor

[C II] 158 μm line detection of the warm ionized medium in the Scutum-Crux spiral arm tangency⋆

T. Velusamy, W. D. Langer, J. L. Pineda, and P. F. Goldsmith

Jet Propulsion Laboratory, California Institute of Technology, 4800 Oak Grove Drive, Pasadena, CA 91109, USA
e-mail: Thangasamy.Velusamy@jpl.nasa.gov

Received 29 March 2012 / Accepted 26 April 2012

ABSTRACT

Context. The *Herschel* HIFI GOT C+ Galactic plane [C II] spectral survey has detected strong emission at the spiral arm tangencies.
Aims. We use the unique viewing geometry of the Scutum-Crux (S-C) tangency near $l = 30°$ to detect the warm ionized medium (WIM) component traced by [CII] and to study the effects of spiral density waves on Interstellar Medium (ISM) gas.
Methods. We compare [C II] velocity features with ancillary H I, ^{12}CO and ^{13}CO data near tangent velocities at each longitude to separate the cold neutral medium and the warm neutral + ionized components in the S-C tangency, then we identify [C II] emission at the highest velocities without any contribution from ^{12}CO clouds, as WIM.
Results. We present the GOT C+ results for the S-C tangency. We interpret the diffuse and extended excess [C II] emission at and above the tangent velocities as arising in the electron-dominated warm ionized gas in the WIM. We derive an electron density in the range of 0.2–0.9 cm^{-3} at each longitude, a factor of several higher than the average value from Hα and pulsar dispersion.
Conclusions. We interpret the excess [C II] in S-C tangency as shock compression of the WIM induced by the spiral density waves.

Key words. ISM: structure – ISM: general – submillimeter: ISM – infrared: ISM

1. Introduction

In spiral galaxies the transition from diffuse to molecular clouds, followed by star formation, and the disruption of molecular clouds and termination of star formation are greatly influenced by the interaction of the interstellar medium (ISM) with spiral density waves. The spiral tangent regions (cf. Vallée 2008; Benjamin 2009) are ideal laboratories to study the interaction of the interstellar gas and spiral density waves in the Milky Way. The tangents provide a unique viewing geometry with sufficiently long path lengths to detect and trace the diffuse atomic or ionized components of the ISM in emission from C^+ and N^+ fine-structure lines, and therefore allow us to study how the diffuse atomic and ionized components are transformed into dense molecular clouds. The 1.9 THz [C II] line ($^2P_{3/2}$–$^2P_{1/2}$ transition of C^+ at 158 μm) emission in the ISM can be excited by collisions with electrons, and atomic and molecular hydrogen in regions with a kinetic temperature $T_k \gtrsim$ 30–40 K. COBE FIRAS observed the strongest [C II] and [N II] emission along the Galactic spiral arm tangencies and Steiman-Cameron et al. (2010) fit the COBE results with four well-defined logarithmic spiral arms in the gaseous component of the ISM. However, COBE's 7° beam and spectrally unresolved lines preclude obtaining detailed information on the scale and properties of the gas in the spiral tangencies, nor whether they arise from PDRs or diffuse gas. The HIFI GOT C+ (Galactic Observations of Terahertz C+) survey of the Milky Way (Langer 2011) also detects the strongest [C II] emission near the spiral arm tangential directions.

The GOT C+ survey consists of ~500 lines-of-sight (LOS) distributed in a volume-weighted sampling of the Galactic disk. The first results based on ~15 LOS (Langer et al. 2010; Velusamy et al. 2010; Pineda et al. 2010) focused on the narrow velocity [C II] features, tracing the distribution and characteristics of the dense atomic and molecular components of the ISM, including the so-called "dark H_2 gas" (H_2 not traced by CO or H I). However, the detection of the more diffuse [C II] emission from the warm ionized medium (WIM) in the HIFI data required completion of the GOT C+ survey and enhanced data processing tools. The WIM is a major Galactic component, with $T_{kin} \sim$ 8000 K, and LOS averaged density $\langle n(e) \rangle \sim 0.03$–$0.10$ cm^{-3}, with volume filling factor $f_v \sim 0.1$ in the plane and increasing to ~0.4 at 1 kpc above the plane (see review by Haffner et al. 2009, based on Hα and pulsar data). The ionization and heating sources of the WIM and its relationship to the other phases of the ISM are not well understood. Carbon radio recombination lines (RRL) have been observed in the ionized gas in H II regions (Quireza et al. 2006) and in extended diffuse regions in the Galactic disk (Roshi et al. 2002). However, detecting and characterizing the 158 μm [C II] emission in the ionized gas is critical to our understanding the Galactic WIM component and its contribution to the [C II] luminosity in galaxies. As shown in Fig. 1 the geometry of the Scutum-Crux (S-C) spiral arm tangent is very favorable to study the structure and kinematics of the WIM component. Here we present the [C II] emission along the S-C spiral arm tangent near Galactic longitude $l = 30°$, indicating higher electron densities, a likely result of compression by density wave shocks.

2. Observations

The observations reported here are a subset of the GOT C+ Galactic plane [C II] survey at 1900.5469 GHz taken with the HIFI instrument (de Graauw et al. 2010) on *Herschel* (Pilbratt et al. 2010). The [C II] spectra were obtained using

⋆ *Herschel* is an ESA space observatory with science instruments provided by European-led Principal Investigator consortia and with important participation from NASA.

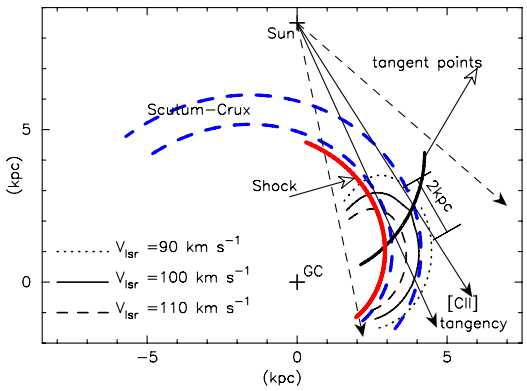

Fig. 1. Schematic of the Scutum-Crux spiral arm (blue dashed lines). The dashed arrows indicate the GOT C+ mapped data presented in this paper, and solid arrows the tangency longitude range traced by [C II] emission. The radial velocity contours, spiral density wave shock (red arc), and the loci of the tangent points (heavy dark arc) are indicated.

the Wide Band Spectrometer (0.17 km s^{-1} velocity resolution over 350 km s^{-1}) in band 7b. For each target Galactic longitude we used the Load CHOP (HPOINT) with a sky reference at $b = \pm 2°$ at each longitude. The data were processed in HIPE-8 using the standard HIFI pipeline. We mitigated the electronic (HEB) and optical band 7b standing waves, following procedures in Higgins (2011): (i) the HEB standing waves are removed with the HEBBaselineFit (subtracting profile- matched off-source spectra using a script provided by the HIFI data processing team); (ii) the optical standing waves are dealt with by subtracting the HEBBaselineFitted OFF-source from the ON-source spectra. We also extracted the OFF-source spectrum to examine and correct for any [C II] spectral contamination in the OFF-source subtraction. The ^{12}CO and ^{13}CO Mopra data (Pineda et al. 2010) were observed at the [C II] LOS, and the H I data were extracted from the VGPS survey (Stil et al. 2006).

3. Results

Figure 1 is a schematic of the Scutum-Crux tangency, which is a 2D cartographic model of the Galactic spiral structure using a 4-arm spiral model (cf. Vallée 2008; Steiman-Cameron et al. 2010). An observational challenge in tracing the distribution and properties of the interstellar gas is to separate the diffuse ionized and atomic components from the dense PDRs and molecular clouds. To do so, we have complemented our [C II] data with observations of the H I 21-cm and CO isotopologue lines to trace the diffuse atomic and molecular gas, respectively. These auxiliary data allow us to isolate the origin of the [C II] emission. Figure 2 summarizes all the GOT C+ [C II] observations and ancillary H I and CO data for the inner Galaxy containing the S-C spiral tangency. The [C II], H I, and CO emission are presented in the form of longitude-velocity ($l - v$) intensity maps. These maps are sparsely sampled in longitude, every 0.9° for $l < 30°$ and 1.3° for $l > 30°$. For easy viewing the intensities at each l are shown by thick bars; the true widths, corresponding to the beam size 12″, 33″ and 60″, respectively for [C II], CO and H I, are much narrower. The S-C tangency is restricted in longitude from 23° to 33° (Fig. 1). In the ($l - v$) maps ($l = 15°$ to 45°) the enhanced [C II] emission at radial velocities >100 km s^{-1} (close to and beyond the tangent velocities) is very prominent at $l = 23°$ to 33°, in striking contrast to other longitudes. It is the strongest in the plane and easily traced at $b = \pm 0.5°$, but marginal at $b = \pm 1.0°$ (Fig. 2a–c).

The overlay of the radial velocities V_{lsr} on the [C II] (l–v) map in Fig. 2a brings out the importance of [C II] as a tracer of spiral arms in the inner Galaxy. The Scutum-Crux (S-C) arm, which is not that well traced by other tracers in these longitudes (cf. Vallée 2008), is well traced by the [C II] emission. However the Sagittarius-Carina arm is only partially traced. This difference between the S-C and the outer arms is primarily because [C II] preferably traces the high FUV environments within Galactic radius ~6 kpc (Pineda et al., in prep.). The loci of the tangent velocities at each longitude (broken line in Figs. 2a, d, and e) were calculated for the Galactic rotation parameters for the first quadrant from H I by Levine et al. (2008, hereafter LHB). The tangent velocities are model dependent, nevertheless, near the S-C tangency both H I and [C II] show emission significantly beyond the tangent velocities, well above the velocities of the ^{12}CO clouds (Figs. 2, 3a). Thus, we can use the CO velocity data to separate the [C II] associated with discrete molecular clouds from that with the warm diffuse atomic and ionized gas components as shown in Fig. 3a. In this [C II] spectrum we note (red arrow) bright anomalous [C II] emission at velocities greater than the tangent velocity (~110 km s^{-1}), which is very distinct from other [C II] spectral features, as it is associated with weak H I while also having no CO counterpart.

To bring out more clearly the exceptional characteristics of the [C II] emission at the S-C tangency velocities on a larger scale we show in Fig. 3b ($l - v$) maps of the highest velocity [C II] and H I components without any CO. To make this display we define $V(\mathrm{CO})_{\mathrm{limit}}$ (in Fig. 3a) for each longitude, as the highest velocity at which discrete ^{12}CO clouds are detected. Then we reconstruct the spectra at each longitude with $V_{lsr} - V(\mathrm{CO})_{\mathrm{limit}}$ as the velocity axis. Therefore, at each longitude emission at $V_{lsr} - V(\mathrm{CO})_{\mathrm{limit}} > 0$ traces the ISM with no CO clouds and the [C II] and H I emission arising in the diffuse atomic/ionized gas. Although at $V_{lsr} - V(\mathrm{CO})_{\mathrm{limit}} > 0$ H I emission is seen at all longitudes, the [C II] is detected only in the longitudes near the S-C tangency with the exception of $l = 36.4°$ (Fig. 3b). We conclude that the relative intensities of [C II], H I and CO emissions are remarkably different for the S-C tangency compared to those for other velocities or longitudes with relatively little H I and no CO. Thus we have isolated a diffuse atomic and/or ionized gas component at the highest velocity along the S-C arm. Assuming circular Galactic rotation, V_{lsr} velocities for the [C II] emission indicate this ionized gas is located in the S-C arm at radial distances 3.6 to 4.2 kpc from the Galactic center across the longitude range $l = 23°$ to 33° (using $r_{sun} = 8.5$ kpc).

4. Discussion

The anomalous excess [C II] emission in the S-C spiral arm tangency is the first example of the direct detection of the large scale Galactic diffuse ionized gas (WIM) by the 158 μm [C II] line emission. From the COBE data only indirect estimates of the fraction of [C II] intensity arising from the WIM could be made by using the [NII] intensities (Steiman-Cameron et al. 2010) due to its poor spatial and spectral resolution. Our *Herschel* HIFI detection of the diffuse ionized gas provides detailed spatial and kinematic information on the nature of this gas component in spiral arms. A possible explanation for this [C II] emission is that it originates from ionized gas that has been compressed, or is being compressed, by the spiral density wave shocks (Fig. 1). We locate the ionized gas traced by [C II] in the spiral tangency using the kinematic distances derived from the observed radial velocities (V_{lsr}). The schematic shown in Fig. 1 demonstrates that the velocity contours derived from the LHB rotation curve for

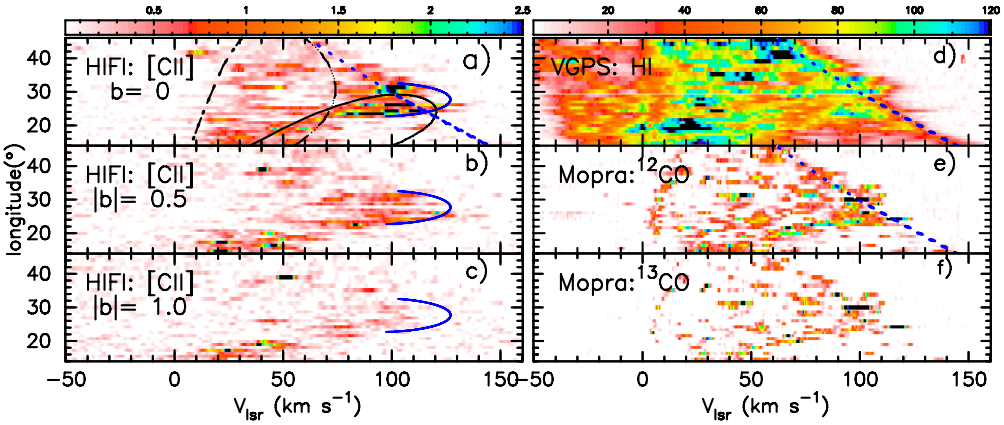

Fig. 2. ($l - v$) maps of [C II], H I and CO emissions in the vicinity of the S-C tangency: **a)–c)** ($l - v$) maps of [C II] intensity at b = 0.0°, ±0.5° and ±1.0°. The arc (blue) indicates the loci of the velocities in the S-C tangent traced by [C II]. The loci of the spiral arm velocities from Galactic rotation are shown in **a)** as contours: Scutum-Crux (solid), Sagittarius-Carina (dashed). **d)–f)**: ($l - v$) intensity maps at b = 0.0° of HI, ^{12}CO(1–0) and ^{13}CO(1–0). The tangent velocity as a function of longitude (see text) is shown by the dashed line (blue). The color bars shown on top represent the [C II] and H I map intensities, $T_{\rm mb}$(K). The highest intensity values (dark blue) in the CO maps are 15 K (^{12}CO) and 4 K (^{13}CO).

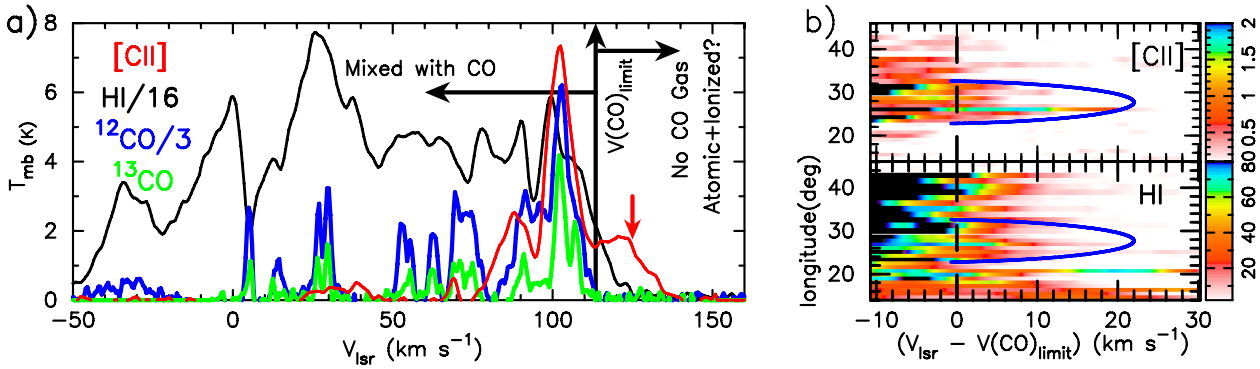

Fig. 3. a) [C II] H I, and CO spectra for LOS: G026.1+0.0, in the S-C tangency. The arrows indicate the velocities of the gases with and without CO (black) and the [C II] excess (red). **b)** ($l - v$) maps of [C II] and H I intensities as function of $V_{\rm lsr} - V({\rm CO})_{\rm limit}$. The color bars shown on the right represent the map intensities, $T_{\rm mb}$(K). The arcs (blue) delineate the longitudes and velocities of the S-C tangency traced by [C II].

$V_{\rm lsr}$ = 90, 100, and 110 km s^{-1} can be used to constrain a linear path length (L) for this large-scale diffuse emission across each longitude. For $l > 30°$ we assume $L \sim 1$ kpc, as these observed radial velocities have no solution in Galactic rotation models. In Table 1 we list the range of radial velocities over which [C II] is detected across the S-C tangency and the inferred path lengths.

We can use the H I and [C II] integrated intensities along each LOS (Table 1) to estimate the LOS averaged densities, $\langle n({\rm H})\rangle$ and $\langle n(e)\rangle$ assuming warm neutral (WNM) and ionized (WIM) conditions, respectively. Defining $\langle n({\rm H})\rangle = N({\rm H})/L$, where $N({\rm H}) = 1.82\times10^{18} I({\rm HI})$ cm^{-2} and L is the path length along the spiral arm tangent, we find $\langle n({\rm H})\rangle$ ~0.05–0.21 cm^{-3} (Table 1) for a range of $N({\rm H}) = 3.3$–5.9×10^{20} cm^{-2}. For the WNM and WIM conditions ($T_{\rm k}$ = 8000 K; Wolfire et al. 2003) the critical density for excitation of [C II] by H atoms is ~1300 cm^{-3}, and for electrons ~45 cm^{-3}. We show below that the required $\langle n({\rm H})\rangle$ to produce the [C II] emission from a WNM is too large compared to the density estimates from H I observations. Following Langer et al. (2010), assuming that this WNM component is uniformly distributed along the tangency, we estimate the minimum required $\langle n({\rm H})\rangle \sim$ 1.7–7.1 cm^{-3} to produce the I(CII) in Table 1 using the corresponding path lengths for each LOS. These densities are factors of 20 to 150 larger than the $\langle n({\rm H})\rangle$ inferred from H I intensities and column densities. Furthermore, in the ($l - v$) maps in Fig. 3b, we detect significant H I emission at $V_{\rm lsr} > V({\rm CO})_{\rm limit}$ at all longitudes, whereas [C II] emission is restricted to longitudes of the S-C tangency. If the [C II] emission were excited only by H collisions we would expect to detect it at all longitudes in proportion to I(HI), which is not observed. Finally, we analyze the possibility of H_2 excitation and find $\langle n({\rm H_2})\rangle \sim$ 5–17 cm^{-3} is needed to produce the observed I(CII). Such low H_2 densities over long path lengths are unrealistic for H_2 formation, especially, given the low $\langle n({\rm H})\rangle$. The observed broad velocity ranges for the [C II] emission over 10° longitude also precludes it originating in compact high density regions. Clearly the [C II] emission is not produced by H or H_2 excitation. Furthermore, in the low resolution ($l - v$) maps of hydrogen RRL, the S-C tangency is evident at these velocities (Alves et al. 2012).

In the diffuse medium the excitation is sub-thermal and the emission is optically thin, therefore the intensity in an ionized gas is given by, $I({\rm CII}) = \int T_A({\rm CII}){\rm d}v = 6.9\times10^{-16} n(e)/n_{\rm cr}(e)\ \exp(-91.3/T) N({\rm C^+})$ (K km s^{-1}), where $n_{\rm cr}(e)$ is the critical de-excitation density. Assuming constant density and temperature along the LOS and fully ionized carbon, we have $N({\rm C^+}) = n({\rm C^+})L$. We can substitute $n({\rm C^+}) = x({\rm C^+})n_{\rm t}$, where $x({\rm C^+})$ is the fractional abundance of carbon, and $n_{\rm t} = n({\rm H^+}) + n({\rm H}) + 2n({\rm H_2})$. Inserting $n(e) = x(e)n_{\rm t}$, and $n_{\rm cr}(e) = 21.4T_3^{0.37}$, where $T_3 = T/1000$, into the equation for I(CII) yields a solution for $n_{\rm t} = 0.32T_3^{0.18}[I({\rm CII})/(x(e)x_{-4}({\rm C^+})L_{\rm kpc})]^{0.5}$, where x_{-4} is in units of 10^{-4} and $L_{\rm kpc}$ is in kpc. In a fully ionized gas $x(e) = 1$ and adopting $x({\rm C^+}) = 2.9\times10^{-4}$ in the

Table 1. [C II] & H I intensities and derived parameters for S-C tangency.

LOS	V_{lsr} km s^{-1}	ΔV km s^{-1}	$L^{\dagger}$ kpc	I(CII) K km s^{-1}	I(HI) K km s^{-1}	$\langle n(\mathrm{HI})\rangle$ cm^{-3}	$\langle n(e)\rangle^{\ddagger}$ cm^{-3}
G23.5+0.0	116	6	0.6	1.8	217	0.21	0.45
G24.3+0.0	131	12	0.8	2.9	186	0.14	0.50
G25.2+0.0	118	12	2.7	5.7	262	0.06	0.38
G26.1+0.0	125	24	2.3	26.5	184	0.05	0.90
G27.0+0.0	114	18	2.9	4.9	548	0.11	0.34
G27.8+0.0	109	7	2.6	1.8	222	0.05	0.22
G28.7+0.0	117	12	1.8	4.0	141	0.05	0.39
G30.0+0.0	112	12	1	3.1	210	0.12	0.46
G31.3+0.0	119	12	1	4.4	325	0.19	0.55
G32.6+0.0	112	12	1	2.7	291	0.17	0.44
average b = 0.0	117	12	1.8	6.7	530	0.17	0.51
average b = 0.5	107	11	2.2	3.3	740	0.20	0.32
average b = 1.0	93	10	3.5	1.5	672	0.12	0.17

Notes. † Constrained by the highest velocity contours in Fig. 1. ‡ For $x(e) = 1$ and $x(\mathrm{C}^+) = 2.9 \times 10^{-4}$.

S-C tangency (appropriate for $R_{\mathrm{Gal}} \sim 4$ kpc, Wolfire et al. 2003), yields $\langle n_{\mathrm{t}}\rangle \sim 0.19 T_3^{0.18} (I(\mathrm{CII})/L_{\mathrm{kpc}})^{0.5}$.

Using this approach, assuming a fully ionized gas, $x(e) = 1$, we calculate $\langle n(e)\rangle = \langle n_{\mathrm{t}}\rangle$ for all LOS (Table 1) for $T_{\mathrm{k}} = 8000$ K. These estimates, assuming uniform conditions, are reasonable considering that $f_v > 0.1$ in the plane implies a WIM LOS filling factor ~0.5 (Haffner et al. 2009). These values are strictly a lower limit if the gas is partially ionized, $x(e) < 1$, but only weakly so, as $\langle n_{\mathrm{t}}\rangle \propto x(e)^{-0.5}$. The electron densities estimated from [C II], $\langle n(e)\rangle$ in Table 1 are in the range of 0.2–0.9 cm^{-3} with a mean ~0.46 cm^{-3} and 1σ scatter of 0.2 cm^{-3}. We can rule out the excess [C II] emission in the S-C tangency as H II regions and their photoionized envelopes. Although, in the $l-v$ map of H II regions there are about 10 within the longitude range 23°–33° of the S-C tangency at velocities above 110 km s^{-1} (Anderson et al. 2009, and references therein), none overlaps the observed [C II] LOS (Table 1). Furthermore, Anderson et al. report that in this region only 20% of the H II regions do not have detections in ^{13}CO, which is likely to be even less for ^{12}CO detections. Thus by excluding all the velocities having detectible ^{12}CO (see Sect. 3), in effect we have excluded the H II regions while identifying the [C II] excess as representing the WIM gas.

The average densities from the [C II] excess, in Table 1, are several times higher than the LOS averaged densities inferred from pulsar dispersion and Hα measurements, $n_{\mathrm{e}} \sim 0.08$ cm^{-3} (Haffner et al. 2009) and we argue that our larger mean value is a result of compression by the WIM-spiral arm interaction. The relatively low H I emission also implies that we are detecting the WIM and not the WNM. Though local variations by a factor 5 over the global mean density of 0.08 cm^{-3} may be present in the WIM, here, in the S-C tangency we detect these high electron densities all along the spiral arm, over a long path length (>1 kpc). Furthermore, that such elevated densities (by factors ~3–11) are detected only at the spiral arm tangency and not beyond is evidence that this enhancement is unique to this location and viewing geometry (Fig. 1). It is, therefore, conceivable that here we are detecting the WIM which is being compressed by its interaction with the gravitational well of the spiral arms and is on the path to becoming WNM. The [C II] emission extends beyond the $V(\mathrm{CO})_{\mathrm{limit}}$ typically to ~12–18 km s^{-1} indicative of the presence of large non-circular velocity components due to shocks in the gas traced by [C II]. This scenario for the shock induced compression and velocities is consistent with the interstellar gas response to spiral pattern speed as seen in hydrodynamical models (Martos et al. 2004). The lack of a smooth distribution in longitude of the WIM all across the S-C tangency as traced by [C II] (Fig. 3b) is possibly the result of a spatially complex gaseous response to an orderly spiral potential (see Yáñez et al. 2008). We also estimate $\langle n(e)\rangle$ averaged over the tangency at $b = 0.0°$, $\pm 0.5°$ ($z = 70$ pc) and $\pm 1.0°$ ($z = 140$ pc) by averaging over all l (from 23° to 33°) and integrating over 10 km s^{-1} above the $V(\mathrm{CO})_{\mathrm{limit}}$. The results (Table 1), in spite of the uncertainties in the path lengths, seem to indicate a trend in the decrease of $\langle n(e)\rangle$ with increasing z, while $\langle n(\mathrm{H})\rangle$ is roughly constant. Such a trend would be consistent with the spiral density shocks being more effective near the plane of the Galaxy.

In this Letter we present the first detection of the WIM in spectrally resolved [C II] 158 μm emission. Future *Herschel*/SOFIA [NII] spectral data will help characterize the WIM. Our interpretation of [C II] excess tracing the WIM in the S-C tangency is further supported by similar detections along other spiral tangencies of S-C at $l \sim 310°$ and Norma-3 kpc including the start of Perseus at $l = 330°$–$342°$ (Langer 2011). It is conceivable that the WIM traced by [C II] at the S-C tangency exists all around the spiral arms, but unlike the tangent direction it is not easy to detect towards other directions due to insufficient path length and velocities blended with other components. Thus it may add significantly to the total [C II] luminosity in galaxies.

Acknowledgements. We acknowledge the helpful comments by the referee. We thank the staffs of the ESA and NASA *Herschel* Science Centers for their help. HIFI has been designed and built by a consortium of institutes and university departments from across Europe, Canada and the United States under the leadership of SRON Netherlands Institute for Space Research Groningen, The Netherlands and with major contributions from Germany, France, and the US. Consortium members are: Canada: CSA, U. Waterloo; France: CESR, LAB, LERMA, IRAM; Germany: KOSMA, MPIfR, MPS; Ireland: NUI Maynooth; Italy: ASI, IFSI-INAF, Osservatorio Astrofisico di Arcetri-INAF; The Netherlands: SRON, TUD; Poland: CAMK, CBK; Spain: Observatorio Astronomico Nacional (IGN), Centro de Astrobiologia (CSIC-INT); Sweden: Chalmers University of Technology MC2, RSS & GARD, Onsala Space Observatory, Swedish National Space Board, Stockholm University Stockholm Obseratory; Switzerland: ETH Zurich, FHNW; USA: Caltech, JPL, NHSC. This work was performed at the Jet Propulsion Laboratory, California Institute of Technology, under contract with the National Aeronautics and Space Administration.

References

Alves, M. I. R., Davies, R. D., Dickinson, C., et al. 2012, MNRAS, submitted
Anderson, L. D., Bania, T. M., Jackson, J. M., et al. 2009, ApJS, 181, 255
Benjamin, R. A. 2009, in IAU Symp., 254, 319
de Graauw, T., Helmich, F. P., Phillips, T. G., et al. 2010, A&A, 518, L6
Haffner, L. M., Dettmar, R.-J., Beckman, Wood, K., et al. 2009, Rev. Mod. Phys., 81, 969
Higgins, D. R. 2011, Advanced Optical Calibration of the Herschel HIFI Heterodyne Spectrometer, Ph.D. Thesis, National Univ. Ireland Maynooth.
Langer, W. D. 2011, in MilkyWay2011, http://mw2011.ifsi-roma.inaf.it/
Langer, W. D., Velusamy, T., Pineda, J. L., et al. 2010, A&A, 521, L17
Levine, E. S., Heiles, C., & Blitz, L. 2008, ApJ, 679, 1288 (LHB)
Martos, M., Yañez, M., Hernandez, X., et al. 2004, J. Korean Astr. Soc., 37, 199
Pilbratt, G. L., Riedinger, J. R., Passvogel, T., et al. 2010, A&A, 518, L1
Pineda, J. L., Velusamy, T., Langer, W. D., et al. 2010, A&A, 521, L19
Quireza, C., Rood, R. T., Balser, D. S., & Bania, T. M. 2006, ApJS, 165, 338
Roshi, D. A., Kantharia, N. G., & Anantharamaiah, K. R. 2002, A&A, 391, 1097
Steiman-Cameron, T. Y., Wolfire, M., & Hollenbach, D. 2010, ApJ, 722, 1460
Stil, J. M., Taylor, A. R., Dickey, J. M., et al. 2006, AJ, 132, 1158
Vallée, J. P. 2008, AJ, 135, 1301
Velusamy, T., Langer, W. D., Pineda, J. L., et al. 2010, A&A, 521, L18
Wolfire, M. G., McKee, C. F., Hollenbach, D., et al. 2003, ApJ, 587, 278
Yáñez, M. A., Norman, M. L., Martos, M. A., et al. 2008, ApJ, 672, 207